Supplementary Materials

Future of the human climate niche

Chi Xu [1,*], *Timothy A. Kohler* [2,3,4,5], *Timothy M. Lenton* [6], *Jens-Christian Svenning* [7], *and Marten Scheffer* [3,8,9,*]

1. *School of Life Sciences, Nanjing University, China*
2. *Department of Anthropology, Washington State University, Pullman, USA*
3. *Santa Fe Institute, Santa Fe, USA*
4. *Crow Canyon Archaeological Center, Cortez, USA*
5. *Research Institute for Humanity and Nature, Kyoto, Japan*
6. *Global Systems Institute, University of Exeter, Exeter, UK*
7. *Center for Biodiversity Dynamics in a Changing World, Department of Bioscience, Aarhus University, Aarhus C, Denmark*
8. *Wageningen University, The Netherlands*
9. *SARAS Institute, Uruguay*

** Corresponding authors: marten.scheffer@wur.nl and xuchi@nju.edu.cn*

www.pnas.org/cgi/doi/10.1073/pnas.1910114117

Materials and Methods

Data sources and pre-processing

We conducted systematic analyses to characterize the human climate niche using global gridded datasets for human population as well as a range of social and environmental variables. We used the current (2015 CE) population data (10-km spatial resolution) available from the History Database of the Global Environment (HYDE 3.1, downloaded from http://themasites.pbl.nl/tridion/en/themasites/hyde/) [1]. Reconstructed population data for mid-Holocene (~6Ky BP), 500y BP and 300y BP are also available from the HYDE 3.1 database. For early periods these population data are hindcast from multiple sources. Empirical archaeological evaluation of these hindcasts is only beginning; non-spatially explicit comparisons between taphonomically corrected frequency distributions of calibrated ^{14}C dates and the HYDE 3.1 estimates show many similar features through time for North America and Australia [2]. The HYDE 3.1 population distributions for 1000 CE are considered sufficiently accurate for the rice cultivation areas of Asia to serve as a starting point for estimating earlier and later methane production from rice cultivation and livestock pastoralism [3].

For mid-Holocene, we also reconstructed the distribution of population density based on direct estimates from archaeology, drawing on the ArchaeoGlobe database, for comparison with the hindcasted HYDE data. The ArchaeoGlobe public data v2.0 [4] and their regions [5] were downloaded from Harvard Dataverse (we also repeated all analyses using the ArchaeoGlobe public data v3.0 that was updated after submitting the manuscript, and the results are highly robust to the updated data). The ArchaeoGlobe public dataset contains estimates of how widespread various adaptation types were in each of 146 regions in each of 10 periods from 10Ky BP to 1850 CE, crowd-sourced by invitation from archaeologists with established expertise in each region. A new dataset was created with the modal commonality categories (possible values are none, minimal [<1%], common [1-20%], and widespread [>20%]) for each of four adaptation types (foraging/hunting/gathering/fishing [FHGH], extensive agriculture [EA], intensive agriculture [IA], and pastoralism [P]) for each region, for the 6Ky BP period. Thirteen regions with no density estimates were coded as missing values. On average there were 4.5 different coders (i.e., estimates of commonality) for each region with non-missing values.

To obtain density estimates for FHGH populations we used effective temperatures estimated for 6Ky BP generated from simulations with the downscaled Global Climate Models from the IPPC Fifth Assessment Report (CMIP5), assigning each ArchaeoGlobe region to one of seven climate classes as defined in Binford (2001 Table 7.02) [6]. We then computed the mean population densities for FHGH populations for each climate zone from Binford's tabulation, and divided these by 100 to get densities/km^2, as follows:

1. polar, .053
2. boreal, .123
3. cool temperate, .421
4. warm temperate, .262
5. subtropical, .374
6. tropical, .374
7. equatorial, .345

Population density estimates for other adaptation types were not indexed by climate zone, and were taken from Hassan (1981: Figure 4.1) [7] as follows: EA (Hassan's "early dry farming") and P, 5 persons/km^2; and IA, 15 persons/km^2.

Finally, we considered the codes "widespread" to equal 30%, "common" to equal 10%, "minimal" to equal 1%, and "none" to equal 0%. For each region, these numbers were summed and divided by 100 to obtain the raising factor necessary to make these sum to 1. Then regionally and adaptationally appropriate population densities could be computed using the raised proportions to admix the "pure" population densities. For example, for a region in the cool temperate zone in which FHGF and EA are both "widespread" and IA and P are absent, each 30% gets raised to 50% and the admixed population density for that zone is computed as $(0.5 \times 0.421) + (0.5 \times 5) = 2.71$.

The projected population data (~15-km resolution) for the time period 2070 under 5 Shared Socioeconomic Pathways (i.e., SSP1-5) were downloaded from the website of the Climate and Global Dynamics Laboratory of the National Center for Atmospheric Research (http://www.cgd.ucar.edu/iam/modeling/spatial-population-scenarios.html) [8].

We examined actual crop production, livestock distribution, and gross domestic product (GDP) to comprehensively characterize human niches in terms of socioeconomic dimensions for the current conditions. The GDP data for the year 2015 are available from a 1-km resolution global GDP dataset compiled by Kummu and Guillaume [9] (downloaded from https://datadryad.org/resource/doi:10.5061/dryad.dk1j0/9 [10]). The actual total crop production data for the year 2000 (10-km resolution) are available from the Global Agro-ecological Zones Data Portal (GAEZ version 3.0, http://gaez.fao.org/) [11]. The livestock data (1-km resolution) for the year 2006 are available from the FAO Gridded Livestock of the World version 2.0 (downloaded from https://livestock.geo-wiki.org/Application/index.php) [12]. We converted the data for different livestock species (including cattle, pig, goat, sheep, duck and chicken) to the standard livestock unit (LSU) using the coefficients from Eurostats (http://ec.europa.eu/eurostat/statistics-explained/index.php/Glossary:Livestock_unit_(LSU)).

The mean annual temperature (MAT) and mean annual precipitation (MAP) data (~1-km resolution) for the mid-Holocene (6Ky BP), current and future (2070) conditions are available from the WorldClim dataset version 1.4 (http://www.worldclim.org) [13]. The climate data for the current conditions (representative of 1960-1990) were generated from interpolated weather station data. The climate data (Table S1) for 6Ky BP and 2070 (averaged for the period 2061-2080) were generated from simulations with the downscaled Global Climate Models (GCMs) from the IPPC Fifth Assessment Report (CMIP5). For the time period 2070 we take into account three Representative Concentration Pathways (i.e., RCP2.6, RCP4.5 and RCP8.5; RCP6.0 was not included in this study because it is close to RCP4.5 by the year 2070) that are used for characterizing different scenarios of greenhouse gas concentration trajectories adopted by the IPCC for its fifth Assessment Report (AR5).

The climate data for 500y BP and 300y BP were reconstructed from the near-surface air temperature (tas) and precipitation (pr) variables in the "past1000" experiment as part of the Palaeoclimate Modeling

Intercomparison Project 3 (PMIP3) [14]. The simulation models used are shown in Table S2 (see https://data.giss.nasa.gov/modelE/ar5/ for model details).

The mean annual NPP data (~1-km resolution) during 2000-2015 retrieved from the MODIS MOD17A3 product are available from the online Data Pool (https://lpdaac.usgs.gov/dataset_discovery/modis/modis_products_table/mod17a3), courtesy of the NASA EOSDIS Land Processes Distributed Active Archive Center (LP DAAC), USGS/Earth Resources Observation and Science (EROS) Center, Sioux Falls, South Dakota. Total exchangeable bases (the sum of HCl-soluble bases including Ca^{2+}, Mg^{2+}, K^{+} and Na^{+}) were used as an indicator of soil fertility [15]. The soil data (1-km resolution) are available from the Harmonized World Soil Database version 1.2 (http://www.fao.org/soils-portal/soil-survey/soil-maps-and-databases/harmonized-world-soil-database-v12) [16].

All spatial data were resampled to a consistent spatial resolution of 0.083 decimal degree (~10 km) for subsequent analyses.

Data analyses

We plotted heat maps in the MAP-MAT space to illustrate the hotspots of human distribution for the past and current conditions (Fig. 1A-C). The heat maps were produced by calculating the mean population density within each bin (sized of 40 mm MAP × 0.5 °C MAT for the current condition in Fig. 1A and 6Ky BP in Fig. 1C; a coarser bin size of ~130 mm MAP × ~1.5 °C MAT was used for Fig. 1B to avoid seriously discontinuous distribution of the data points caused by the coarse resolution of the climate data for 500y BP) in the state space, and then the result was smoothed by a low-pass filter with 5 × 5 bins. To account for potential bias induced by sparse sampling, we excluded the bins with sparse data points (i.e. data point densities lower than 1st percentile, <~30 data points). Using the same approach, we also plotted the current distributions for crop production, livestock unit, GDP, soil fertility and NPP, respectively (Fig. 2D-F, H-I). Point density in each bin (before smoothing) in the climate state space was shown in Fig. 2G (for illustration, point density was log-transformed due to its highly skewed distribution).

We plotted the running mean of population density, crop production, livestock unit and GDP against MAT (with a bin size of 2 °C) and MAP (with a bin size of 200 mm) for the current condition (Fig. S1). We then compared the running mean of population density (normalize to sum unity) against MAT for the past, current and future conditions (Fig. 2A, Fig. S6). To account for uncertainties of reconstructed past climate and projected future climate conditions, we calculated the 5th and 95th percentiles of the running mean curves using all ensemble data from the climate models. For the current condition, we also conducted an uncertainty analysis by including another population dataset of 2015 (The Gridded Population of the World, Version 4: Population Density Adjusted to Match 2015 Revision of UN WPP Country Totals [17]), and two other climate datasets (the Climate Research Unit's High-resolution gridded datasets v4.02 [18] and the TerraClimate dataset [19]) for MAT and MAP representative of 1960-1990. The 5th and 95th percentiles were also calculated for the running mean curves generated from all combinations of climate and population datasets (2 population datasets × 3 climate datasets, note that in this particular case with sparse data, the 5th-95th percentile envelope is equivalent to the minimum-maximum envelope).

We modeled the realized human climate niche based on double-Gaussian fitting of the running mean of the current population distribution against MAT (Fig. 2A, blue dashed curve). We then projected the modelled niche to the past (6Ky BP) and future (2070, under different RCPs) climate conditions to illustrate the geographic shift of human climate niche over time (Fig. 3, Figs. S8-S10). To test for the robustness of adding precipitation as an additional dimension of human climate niche, we also projected the smoothed human distribution in terms of MAT and MAP (Fig. 1A) to the past and future climates (Fig. S10).

To quantify the geographic shift of human climate niche in terms of MAT, we calculated percentage proportion of summed niche gain or loss (Fig. S12). By multiplying the projected world's total population by the proportion of displaced human niche, we estimated the number of people who would need to be displaced if the climate niche remained unchanged by the year 2070 in different demographic (SSPs) and climate (RCPs) scenarios (Fig. S13, Table S3). Using this result we also estimated the number of potentially displaced people per degree warming (on average) relative to the pre-industrial period in different SSPs based on the warming trajectories [20] of RCP2.6 and RCP8.5 (Fig. S14). We also calculated the mean geographic latitude of the human climate niche for different time periods to demonstrate the shift of niche towards high latitudes in the future ~50 years (Fig. S11).

For the different time periods, we quantified mean temperature experienced by an average human as a function of global mean of MAT weighted by population density. For 2070, when absent of migration, we considered different scenarios of climate change (RCP2.6, RCP4.5 and RCP8.5) and population growth (zero growth relative to the 2015 condition, and SSP1-5). We included different climate models (Table S1, S2) to account for uncertainties of climate change.

The scripts for all computations and the data used in the analyses are deposited in Dryad (https://doi.org/10.5061/dryad.fj6q573q7).

Table S1. The downscaled 1-km Global Climate Models used (×) for calculating climate data for the time periods 2070 and mid-Holocene. See the WorldClim website (http://www.worldclim.org/) for details.

Model	code	2070			Mid Holocene (6Ky BP)
		RCP2.6	RCP4.5	RCP8.5	
ACCESS1-0	AC	-	×	×	-
BCC-CSM1-1	BC	-	×	×	×
CCSM4	CC	×	×	×	×
CESM1-CAM5-1-FV2	CE	-	×	-	-
CNRM-CM5	CN	×	×	×	×
GFDL-CM3	GF	×	×	×	-
GFDL-ESM2G	GD	×	×	-	-
GISS-E2-R	GS	×	×	×	-
HadGEM2-AO	HD	×	×	×	-
HadGEM2-CC	HG	-	×	×	×
HadGEM2-ES	HE	×	×	×	×
INMCM4	IN	-	×	×	-
IPSL-CM5A-LR	IP	×	×	×	×
MIROC-ESM-CHEM	MI	×	×	×	-
MIROC-ESM	MR	×	×	×	×
MIROC5	MC	-	×	×	-
MPI-ESM-LR	MP	×	×	×	-
MRI-CGCM3	MG	×	×	×	×
NorESM1-M	NO	×	×	×	-
MPI-ESM-P	ME	-	-	-	×

Table S2. The Global Climate Models used for calculating climate data for the time periods 500y BP and 300y BP. To account for volcanic forcing, the ensemble members for GISS-E2-R were r1i1p121, r1i1p1221, r1i1p124, r1i1p125, r1i1p127, and r1i1p128, with r1i1p1 for all other models. See the model website (https://data.giss.nasa.gov/modelE/ar5/) for details.

Model	Ensemble member	Original spatial resolution (degree)	Reference
CSIRO-Mk3L-1-2	r1i1p1	5.625 ×3.18	[21]
GISS-E2-R	r1i1p121, r1i1p1221, r1i1p124, r1i1p125, r1i1p127, r1i1p128	2.5 × 2	[22]
HadCM3	r1i1p1	3.75 × 2.5	[23]
IPSL-CM5A-LR	r1i1p1	3.75 × 1.89	[24]
MPI-ESM-P	r1i1p1	1.875 × 1.86	[25]

Figure S1. Running mean of population density (HYDE 3.1), crop production, livestock, and GDP against mean annual temperature (MAT) and mean annual precipitation (MAP) from the WorldClim dataset for the current condition. All data were normalized to sum unity. The consistent optima of the socioeconomic variables mark a global realized human climate niche.

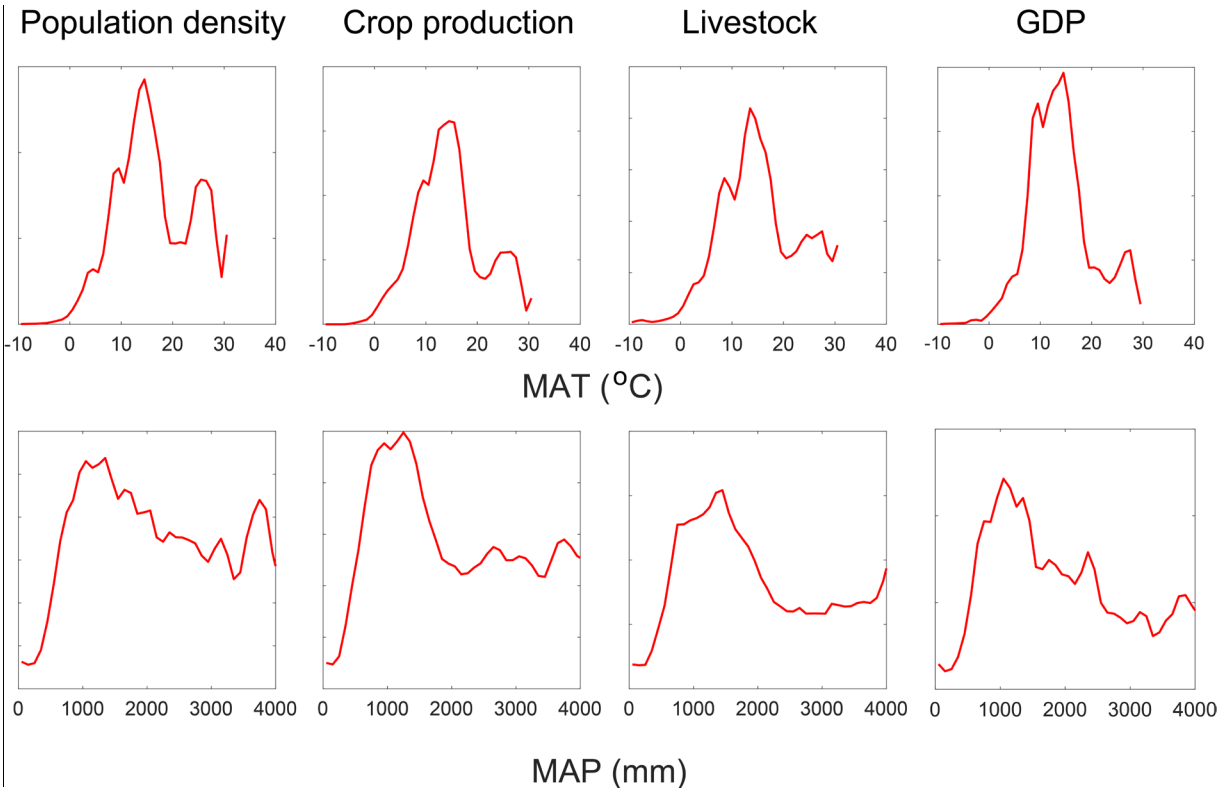

Figure S2. The exclusion of Indian monsoon region (right column) in comparison to all global areas (left column) reveals that the population density mode around ~20-25 °C corresponds largely to the Indian monsoon region. Upper row: running mean of population density (solid curves with bands representing the minimum-maximum envelope) and fitted double Gaussian niche (dashed curves) using the method in Fig. 2; lower row: hot spots of population density in the MAT-MAP space using the method for Fig. 1 (the red-yellow-blue gradient represents population density from high to low).

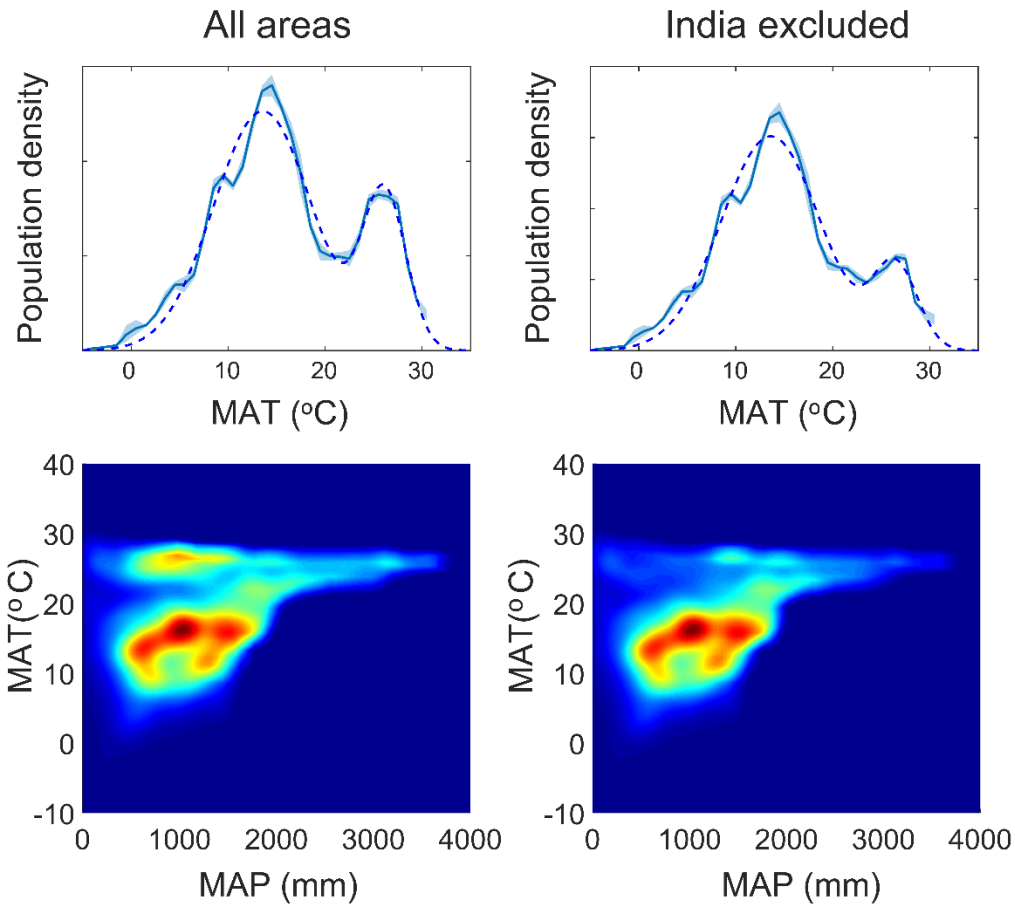

Figure S3. Mean temperature experienced by a human being in different periods. Boxplots and data points (gray dots) are shown for the ensemble of climate and population reconstructions. Different scenarios of climate (RCP2.6, RCP4.5 and RCP8.5) and population growth (zero growth, and SSP1-5) were considered. Reconstructed population data based on the HYDE 3.1 (HY) and ArchaeoGlobe (AG) database were used for 6Ky BP.

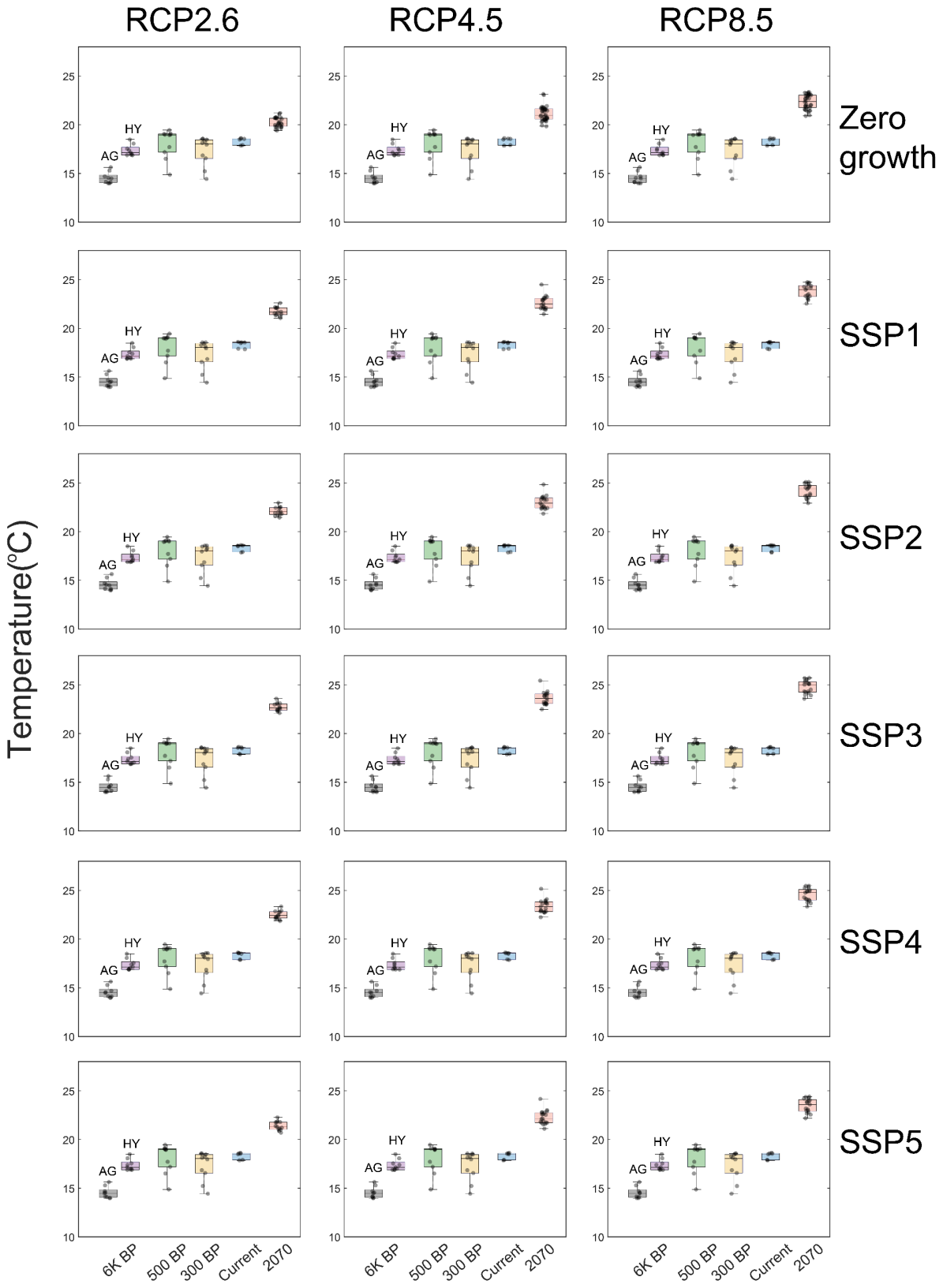

Figure S4. Mean annual temperatures between 17 and 22 °C represent a mode of the projected human temperature niche in 2070 following the RCP 8.5 and SSP3 scenarios (the left-hand mode of the red curve in Fig. S7). In the current climate, such conditions are distributed in the gray areas, but are projected to change to the shaded areas in 2070 (RCP 8.5). Background colors represent the current mean annual temperatures.

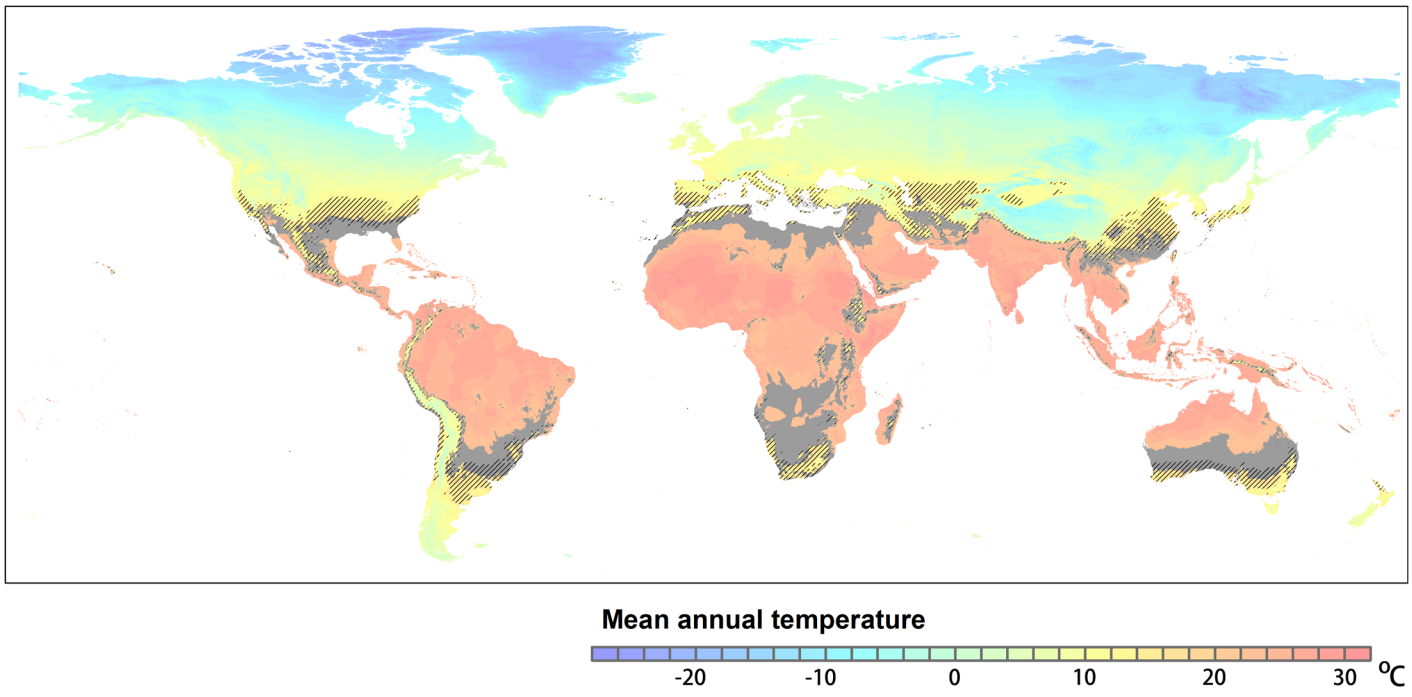

Figure S5. Global distribution of human population densities (A) as compared to the projected population distribution in 2070 following the SSP3 scenario (B). Note differences in upper bound of largest bin.

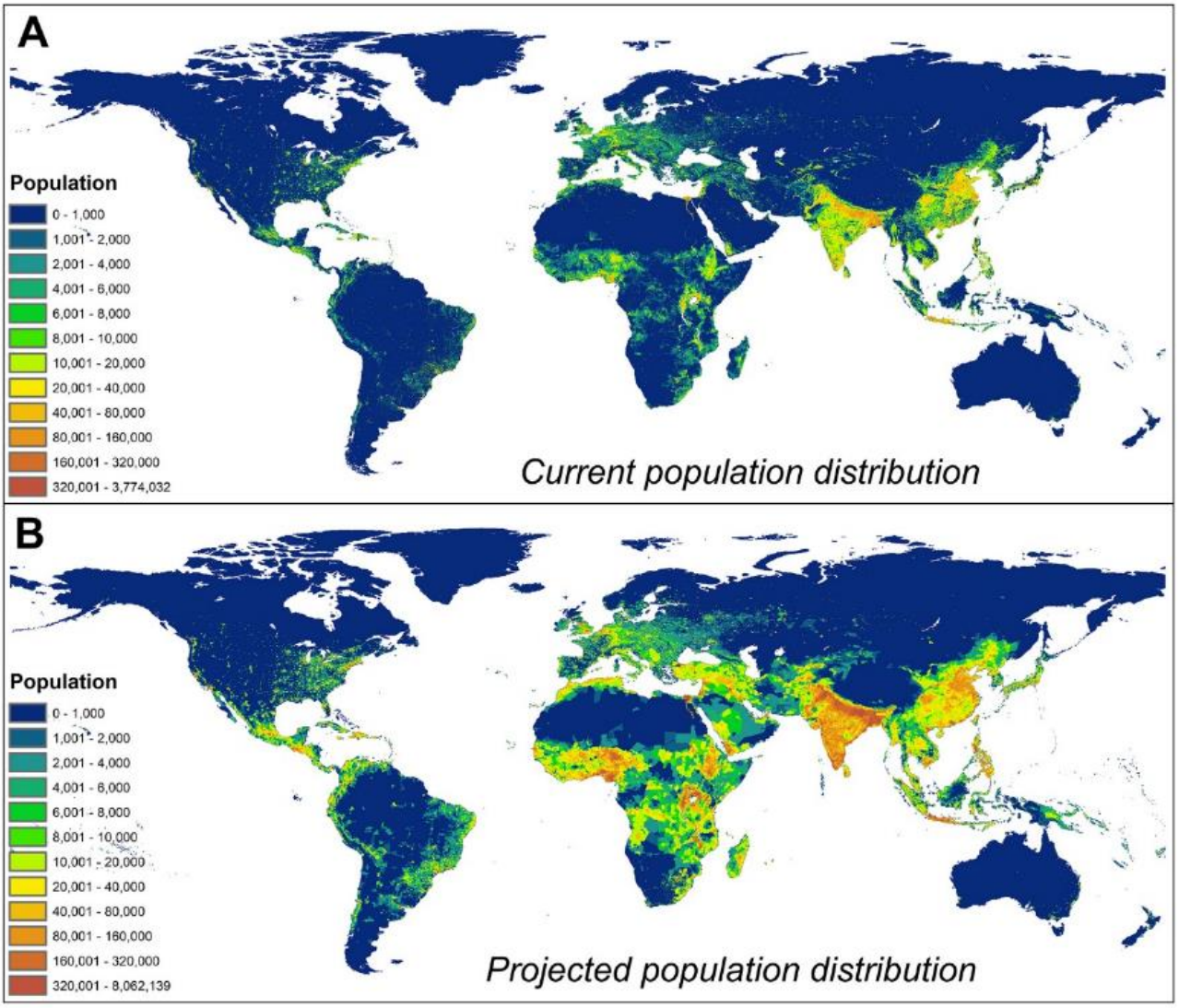

Figure S6. Current and past human population densities (normalized to sum unity) as a function of mean annual temperature (MAT), contrasted to the projected situation in 2070 (red). Different scenarios of climate (RCP2.6, RCP4.5 and RCP8.5) and population growth (zero growth, and SSP1-5) were considered. Bands represent 5th and 95th percentiles of the ensemble of climate and population reconstructions. Reconstructed population data based on the HYDE 3.1 (HY) and ArchaeoGlobe (AG) database were used for 6Ky BP.

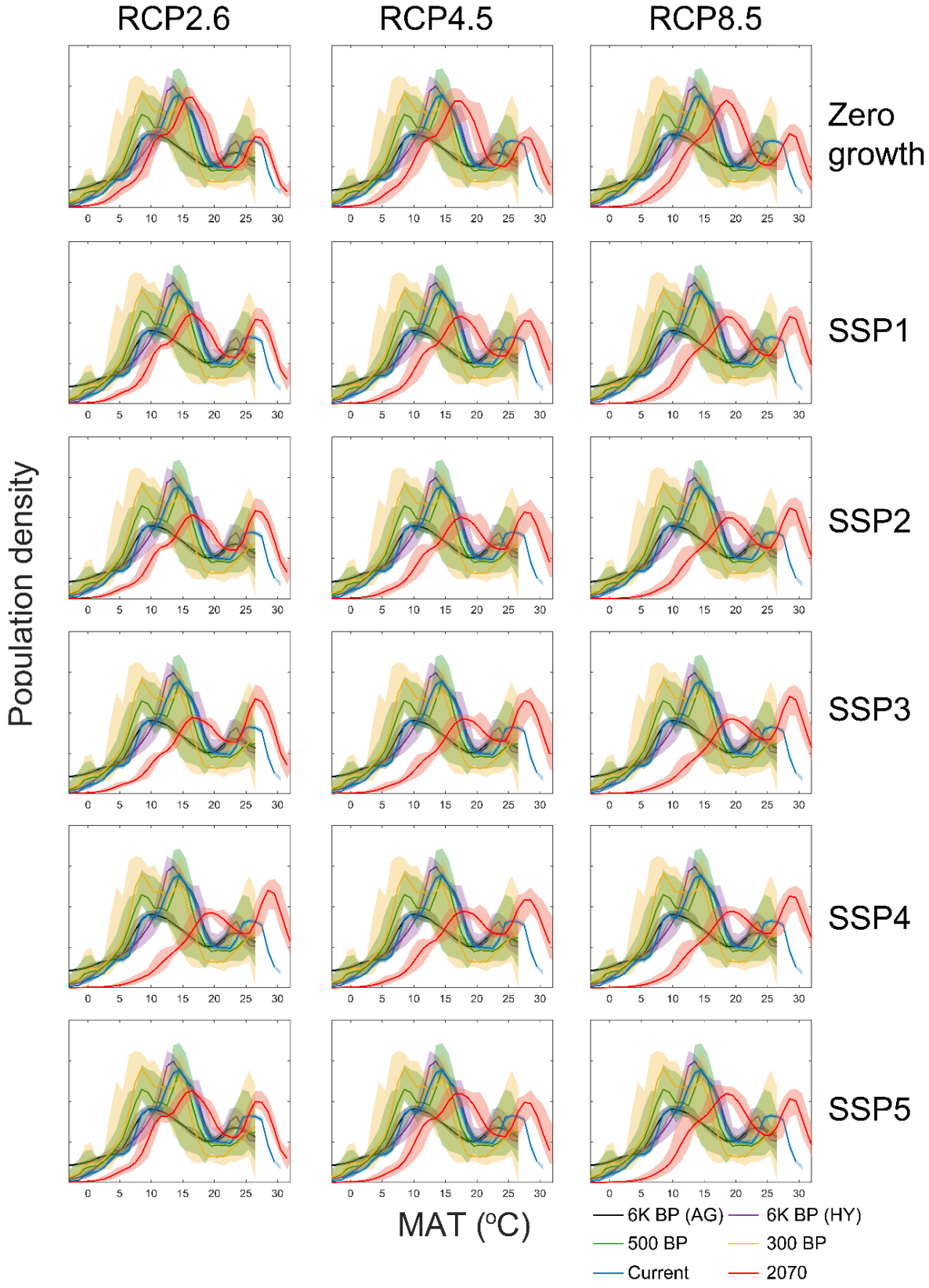

Figure S7. Past and current human niche (fitted by double Gaussian models) in terms of mean annual temperature (MAT), contrasted to the projected situation in 2070 (red). Bands represent 5th and 95th percentiles of the ensemble of climate and population reconstructions. Different scenarios of climate (RCP2.6, RCP4.5 and RCP8.5) and population growth (zero growth, and SSP1-5) were considered. Bands represent 5th and 95th percentiles of the ensemble of climate and population reconstructions. Reconstructed population data based on the HYDE 3.1 (HY) and ArchaeoGlobe (AG) database were used for 6Ky BP.

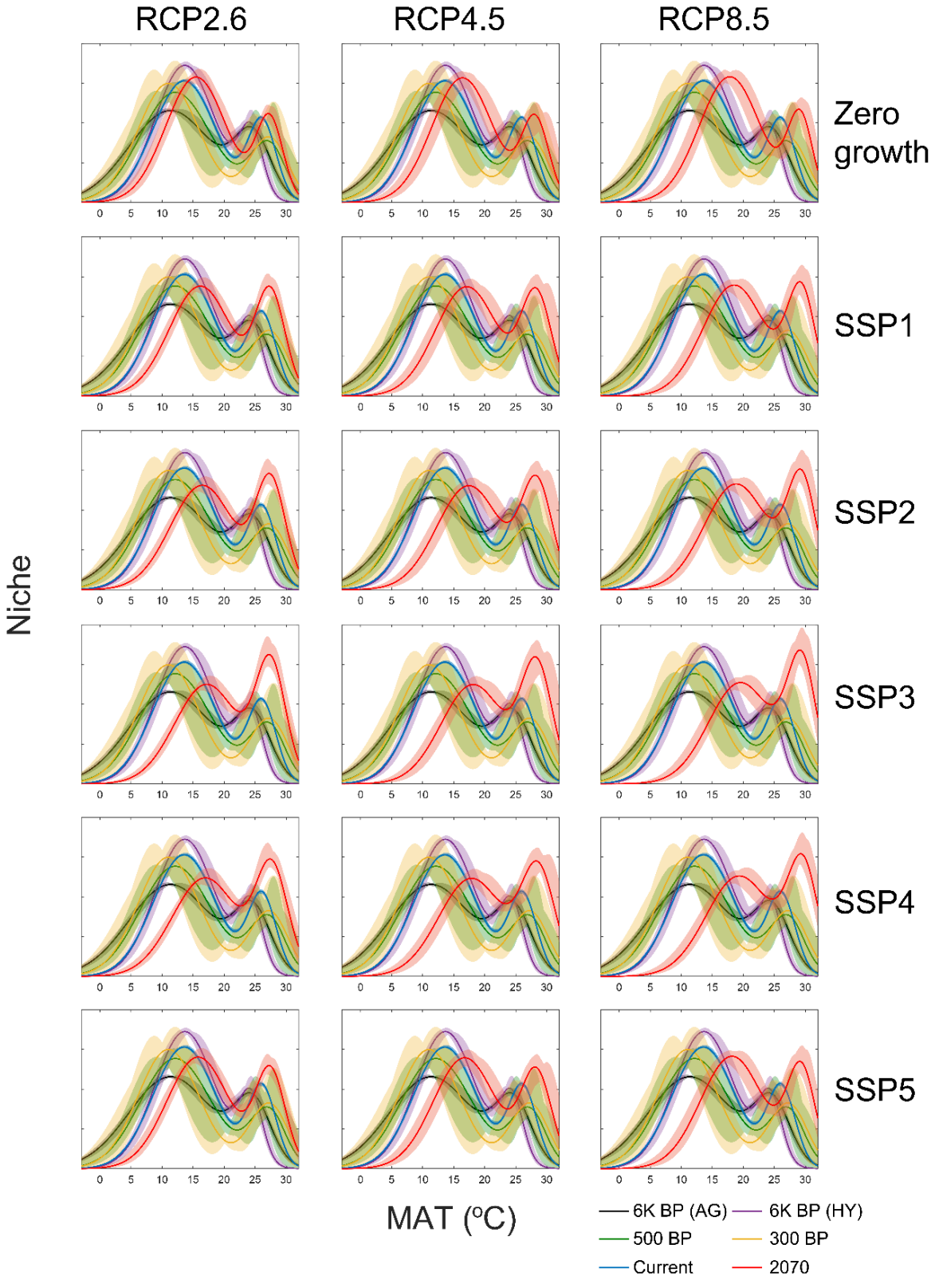

Figure S8. Geographical hotspots of the modeled human temperature niche are similar between 6Ky BP and current conditions. The niche was fitted by double Gaussian models based on the past population and climate conditions, using the gray (panel A, based on reconstructed ArchaeoGlobe population data), purple (panel B, based on reconstructed HYDE population data), and blue (panel C, projecting the current niche to the past climate, assuming that the niche would remain unchanged) curves in Fig. S7. The current niche map in Fig. 4A is also shown in panel D for comparison. The areas outside 90 (black hatched), 95 (blue hatched) and 99 (red hatched) percentiles of suitability are shown.

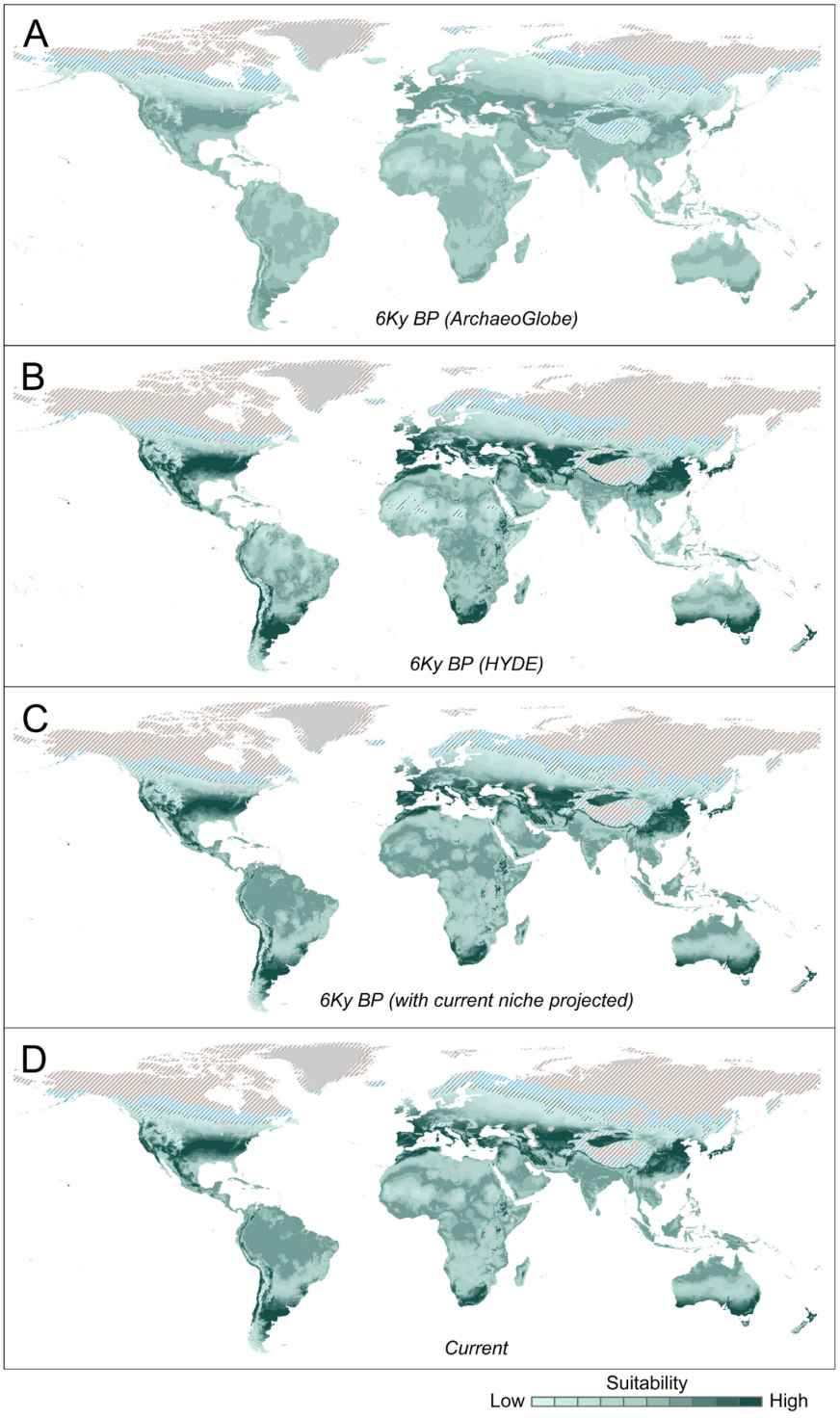

Figure S9. The geographical position (left column) and displacement (right column) of the human temperature niche projected on the past (6Ky BP) and 2070 climate (under RCP 2.6, RCP 4.5 and RCP 8.5, respectively). The maps in the left column represent relative human distributions (summed to unity) for the imaginary situation that humans would be distributed over temperatures following the stylized double Gaussian model fitted to the modern data (the blue dashed curve in Fig. 2A). The areas outside 90 (black hatched), 95 (blue hatched) and 99 (red hatched) percentiles of suitability are shown. The maps in the right column represent geographic displacement of the human niche relative to the current situation (+: gain, -: loss). Note that the 6Ky BP map (same as Fig. S8C) is generated by projecting the modern human climate niche to the past climate, assuming the human niche would remain unchanged over time.

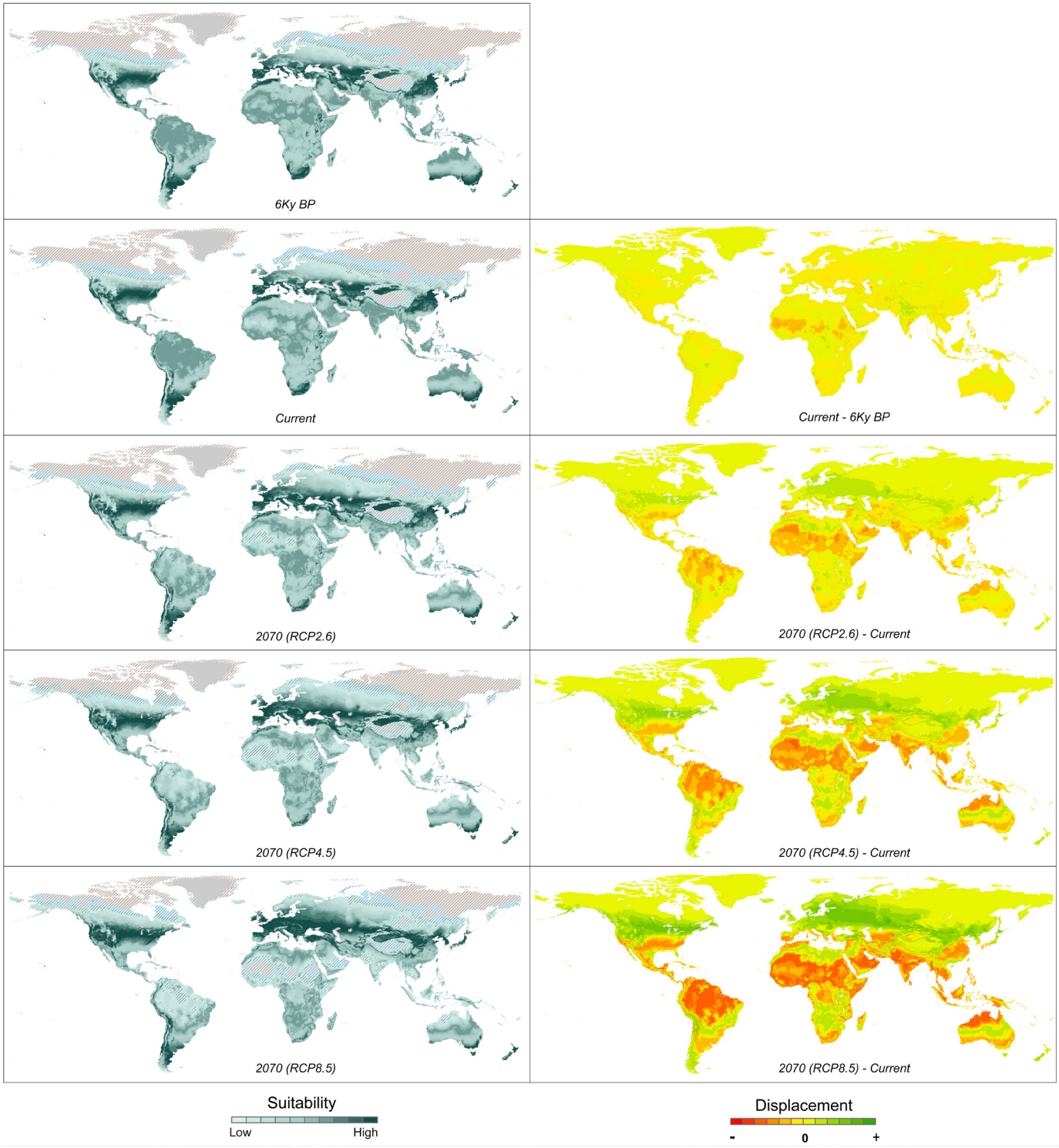

Figure S10. The geographical position (left column) and displacement (right column) of the human niche (relative to available combinations of mean annual temperature and precipitation) projected on the past (6Ky BP) and 2070 climate (under RCP 2.6, RCP 4.5 and RCP 8.5, respectively). The maps in the left column represent relative human distributions (summed to unity) for the imaginary situation that humans would be distributed following the current conditions of mean annual temperature and precipitation (the smoothed surface in Fig. 1A). The areas outside 90 (black hatched), 95 (blue hatched) and 99 (red hatched) percentiles of suitability are shown. The maps in the right column represent geographic displacement of the human niche relative to the current situation (+: gain, -: loss). Note that the 6Ky BP map is generated by projecting the modern human climate niche to the past climate, assuming the human niche would remain unchanged over time.

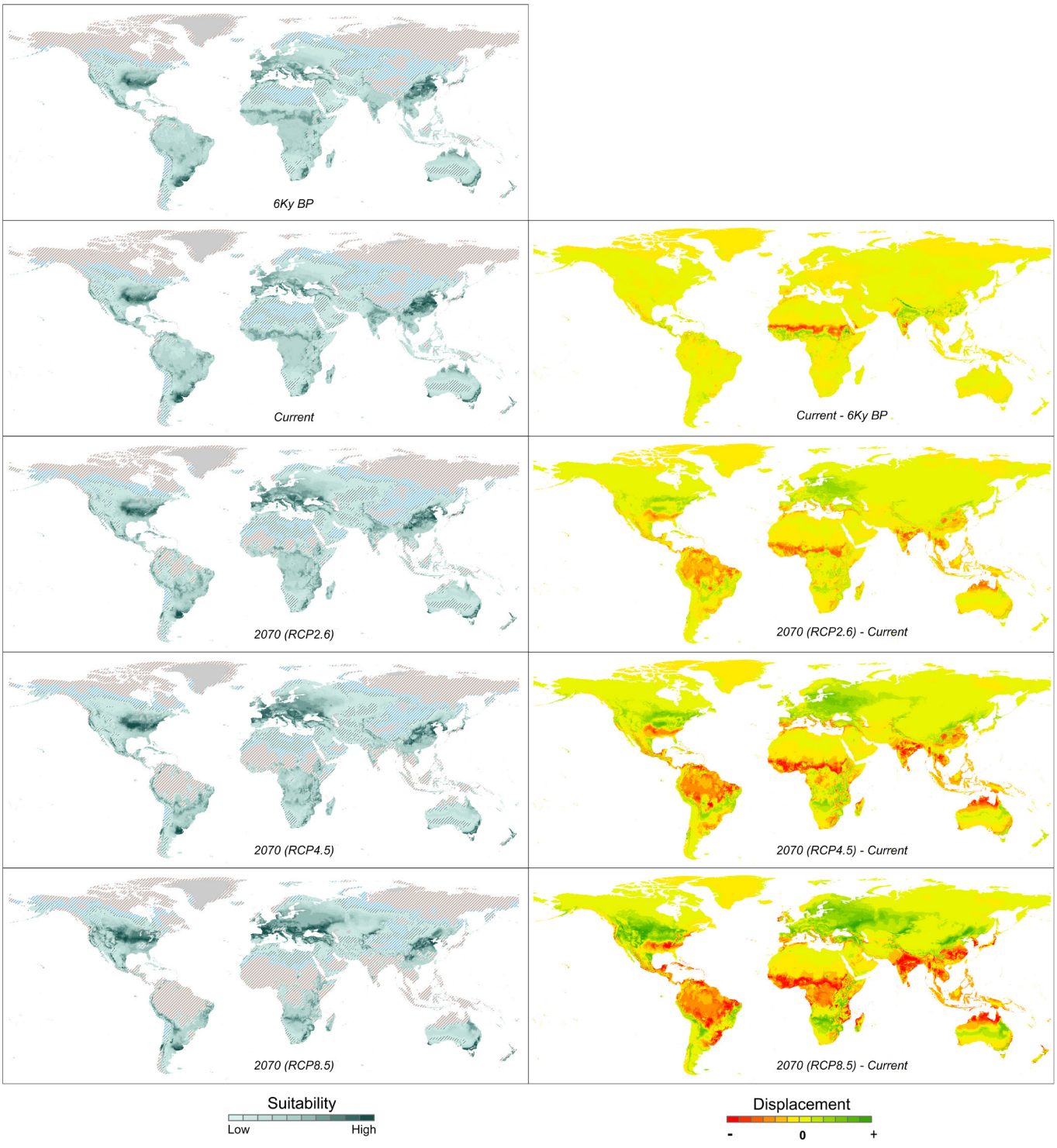

Figure S11. Mean absolute geographic latitude of realized human climate niche in the past ~6000 years (from mid-Holocene), current and the future ~50 years (by the year 2070, if we were to keep the same climate niche, i.e., the distribution relative to mean annual temperature depicted in Fig. 2A). Boxplots and data points (gray dots) are shown for the ensemble of climate models (and 2 population datasets for the current conditions). For 6Ky BP, we reconstructed the niche using the ArchaeoGlobe (the AG box) and the HYDE (the HY box) population data using the gray and purple curves in Fig. S7, respectively; we also projected the modern human niche (the blue curves in Fig. S7) to the past climate (the PMNP box), assuming the human niche would remain unchanged over time.

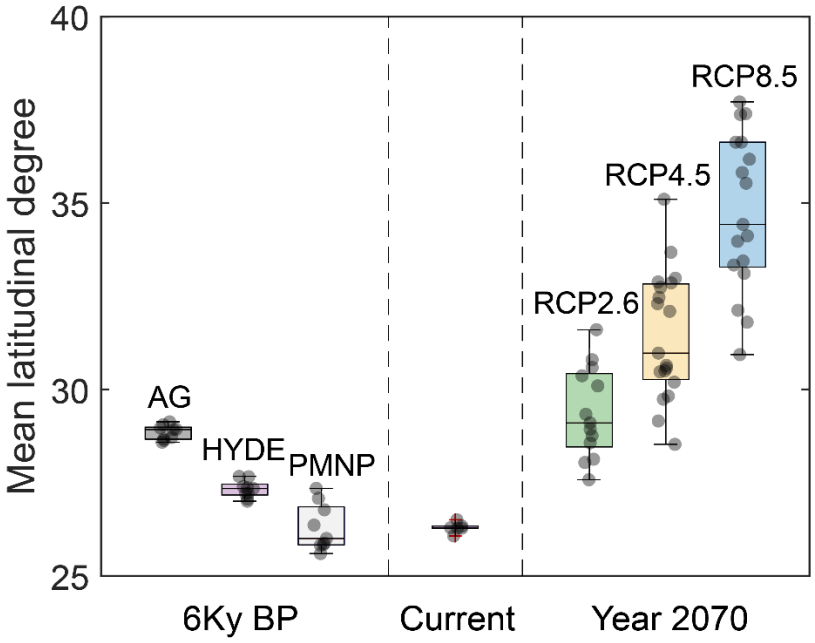

Figure S12. Estimated percentage geographical displacement of human climate niche in the past ~6000 years (since mid-Holocene) and the future ~50 years (by the year 2070 under different RCPs, if we were to keep the same climate niche, i.e., the distribution relative to mean annual temperature depicted in Fig. 2A). Boxplots and data points (gray dots) are shown for the ensemble of climate models. For 6Ky BP, we reconstructed the niche using the ArchaeoGlobe (the AG box) and the HYDE (the HY box) population data using the gray and purple curves in Fig. S7, respectively; we also projected the modern human niche (the blue curves in Fig. S7) to the past climate (the PMNP box), assuming the human niche would remain unchanged over time.

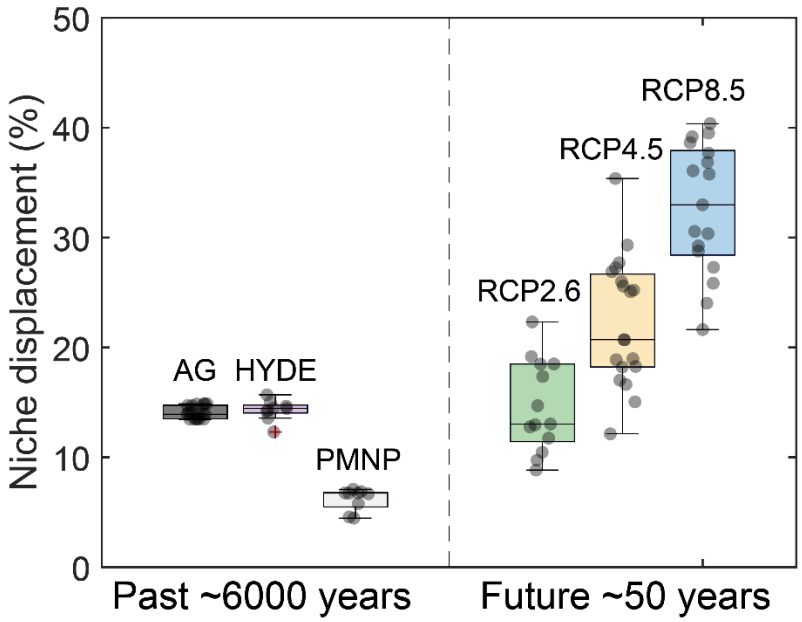

Figure S13. Number of people who would need to be displaced in different demographic and climate scenarios if we were to keep the same climate niche (the distribution relative to mean annual temperature depicted in Fig. 2A) in the future ~ 50 years. Boxplots and data points (gray dots) are shown for the ensemble of climate models.

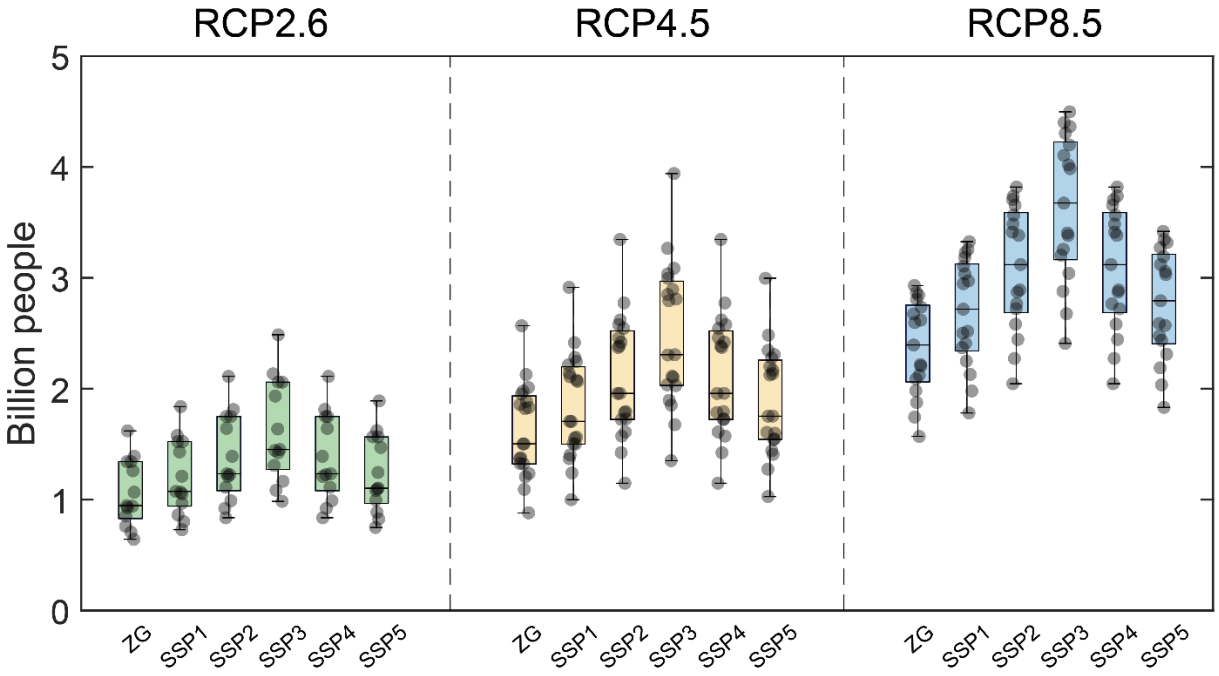

Table S3. World population and temperature rise (relative to the pre-industrial baseline) projected by different demographic and climate scenarios around the year 2070, and number (mean ± std for the ensemble of climate models) of people who would need to be displaced in different demographic and climate scenarios if we were to keep the same climate niche (the distribution relative to mean annual temperature depicted by the blue dashed curve in Fig. 2A).

Demographic scenario (Shared Socio-economic Pathways, SSPs)	**World population growth (billion)**	**World population size (billion)**	**Climate scenario**		
			RCP 2.6	**RCP 4.5**	**RCP 8.5**
			mean projected global temperature rise of ~1.5 °C	-	mean projected global temperature rise of ~3.2 °C
			Displaced people (billion)	**Displaced people (billion)**	**Displaced people (billion)**
Zero growth	0.00	7.26	1.06±0.30	1.62±0.42	2.37±0.43
SSP1	0.98	8.24	1.20±0.34	1.84±0.48	2.69±0.49
SSP2	2.20	9.46	1.38±0.39	2.12±0.55	3.09±0.56
SSP3	3.88	11.14	1.63±0.46	2.49±0.65	3.64±0.66
SSP4	2.20	9.46	1.38±0.39	2.12±0.55	3.09±0.56
SSP5	1.21	8.47	1.24±0.35	1.89±0.49	2.76±0.50

Figure S14. Number of people who would need to be displaced by the year 2070 per Celsius degree warming relative to the pre-industrial period in different demographic and climate scenarios if we were to keep the same climate niche (the distribution relative to mean annual temperature depicted by the blue dashed curve in Fig. 2A). Boxplots and data points (gray dots) are shown for the ensemble of climate models.

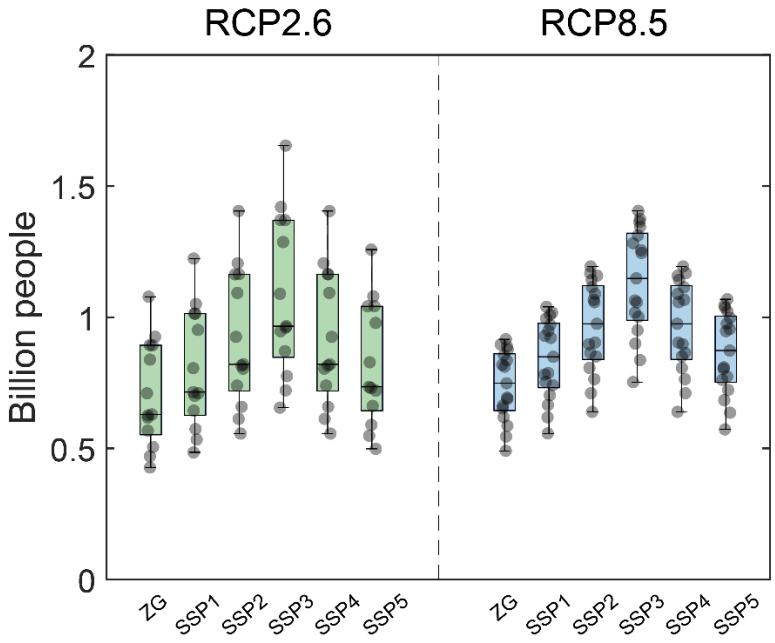

References

1 Klein Goldewijk, K., Beusen, A. & Janssen, P. Long-term dynamic modeling of global population and built-up area in a spatially explicit way: HYDE 3.1. *The Holocene* **20**, 565-573 (2010).

2 Chaput, M. A. & Gajewski, K. Radiocarbon dates as estimates of ancient human population size. *Anthropocene* **15**, 3-12 (2016).

3 Fuller, D. Q. *et al.* The contribution of rice agriculture and livestock pastoralism to prehistoric methane levels: An archaeological assessment. *The Holocene* **21**, 743-759 (2011).

4 Stephens, L. *ArchaeoGLOBE Public Data*. (Harvard Dataverse, 2019).

5 Stephens, L. *ArchaeoGLOBE Regions*. (Harvard Dataverse, 2018).

6 Binford, L. R. *Constructing Frames of Reference: An Analytical Method for Archaeological Theory Building Using Hunter-Gatherer and Environmental Data Sets*. (University of California Press, 2001).

7 Hassan, F. A. *Demographic Archaeology*. (New York: Academic Press, 1981).

8 Jones, B. & O'Neill, B. Spatially explicit global population scenarios consistent with the Shared Socioeconomic Pathways. *Environmental Research Letters* **11**, 084003 (2016).

9 Kummu, M., Taka, M. & Guillaume, J. H. Gridded global datasets for Gross Domestic Product and Human Development Index over 1990–2015. *Scientific Data* **5**, 180004 (2018).

10 Kummu, M., Taka, M. & Guillaume, J. H. A. (Dryad Data Repository, 2018).

11 FAO/IIASA. *Global Agro-ecological Zones (GAEZ v3.0)*. (2011).

12 Robinson, T. P. *et al.* Mapping the global distribution of livestock. *PloS One* **9**, e96084 (2014).

13 Hijmans, R. J., Cameron, S. E., Parra, J. L., Jones, P. G. & Jarvis, A. Very high resolution interpolated climate surfaces for global land areas. *International Journal of Climatology* **25**, 1965-1978 (2005).

14 Braconnot, P. *et al.* Evaluation of climate models using palaeoclimatic data. *Nature Climate Change* **2**, 417-424 (2012).

15 Huston, M. A. Precipitation, soils, NPP, and biodiversity: resurrection of Albrecht's curve. *Ecol Monogr* **82**, 277-296 (2012).

16 FAO/IIASA/ISRIC/ISSCAS/JRC. Harmonized world soil database (version 1.2). *FAO, Rome, Italy and IIASA, Laxenburg, Austria* (2012).

17 Center for International Earth Science Information Network (CIESIN)—Columbia University. Gridded population of the world, version 4 (GPWv4): population density (2016).

18 Mitchell, T. D. & Jones, P. D. An improved method of constructing a database of monthly climate observations and associated high-resolution grids. *International Journal of Climatology* **25**, 693-712 (2005).

19 Abatzoglou, J. T., Dobrowski, S. Z., Parks, S. A. & Hegewisch, K. C. TerraClimate, a high-resolution global dataset of monthly climate and climatic water balance from 1958–2015. *Scientific Data* **5**, 170191 (2018).

20 Meinshausen, M. *et al.* The RCP greenhouse gas concentrations and their extensions from 1765 to 2300. *Climatic Change* **109**, 213 (2011).

21 Phipps, S. *et al.* The CSIRO Mk3L climate system model version 1.0–Part 2: Response to external forcings. *Geoscientific Model Development* **5**, 649-682 (2012).

22 Schmidt, G. A. *et al.* Configuration and assessment of the GISS ModelE2 contributions to the CMIP5 archive. *Journal of Advances in Modeling Earth Systems* **6**, 141-184 (2014).

23 Gordon, C. *et al.* The simulation of SST, sea ice extents and ocean heat transports in a version of the Hadley Centre coupled model without flux adjustments. *Climate Dynamics* **16**, 147-168 (2000).

24 Dufresne, J.-L. *et al.* Climate change projections using the IPSL-CM5 Earth System Model: from CMIP3 to CMIP5. *Climate Dynamics* **40**, 2123-2165 (2013).

25 Stevens, B. *et al.* Atmospheric component of the MPI-M Earth system model: ECHAM6. *Journal of Advances in Modeling Earth Systems* **5**, 146-172 (2013).